

## The metallicity dilution in local massive early-type galaxies

YU-ZHONG WU<sup>1</sup> AND WEI ZHANG<sup>1</sup>

<sup>1</sup>CAS Key Laboratory of Optical Astronomy, National Astronomical Observatories, Beijing, 100101, China

### ABSTRACT

We derive a sample of 114 Baldwin-Phillips-Terlevich diagram - star formation (BPT-SF) and Wide-field infrared Survey Exploer - low star formation rate (WISE-LSFR) early-type galaxies (ETGs) by utilizing the criterion  $W2-W3 < 2.5$  (where  $W2$  and  $W3$  are the wavelengths of 4.6 and 12  $\mu m$  in the WISE four bands) and cross-matching the *Galaxy Zoo* 1 and the catalog of the Sloan Digital Sky Survey Data SDSS Release 7 MPA-JHU emission-line measurements. We find that  $\sim 28\%$  of our ETGs exhibit a metallicity that is at least 2 standard deviation (0.26 dex) below the mass-metallicity (MZ) relation of star-forming galaxies (SFGs) from the SDSS. We demonstrate that almost all of our ETGs locate below the “main sequence” of SFGs. We find that these ETGs with larger metallicity deviation from the MZ relation tend to have lower SFR and redder color. By exploring the dilution properties of these massive ETGs, we report that the dilution effect may be mainly attributed to the inflow of metal-poor gas from mergers/interaction or the intergalactic medium.

*Keywords:* Early-type galaxies — Galaxy abundances — Star formation

### 1. INTRODUCTION

The gas-phase metallicity of the inter-stellar medium (ISM) of galaxies is a key parameter in galaxy formation and evolution, and it is regulated by injection and mixing of metals produced by star formation (SF), inflow of low-metallicity gas, outflow of enriched metallicity gas, and gas accretion from the inter-galactic medium (IGM). A tight correlation between the stellar mass and metallicity of star-forming galaxies (SFGs) was first discovered by Lequeux et al. (1979), and this was later confirmed by observations of a large sample from large surveys (such as the Sloan Digital Sky Survey, SDSS, York et al. 2000; Tremonti et al. 2004, T04).

Early-type galaxies (ETGs) are often regarded as “red and dead” systems at the end of galaxy evolution, where new stars are no longer forming. However, recent years have shown that they are, in fact, complicated objects. The presence of recent or ongoing star formation (SF) in some ETGs has been demonstrated by numerous observations (Yi et al. 2005; Kaviraj et al. 2007; Thilker et al. 2010; Belli et al. 2017), and this SF may originate from various sources.

The ultraviolet (UV) observation serves as a reliable tracer of recent SF in ETGs. The results from *Galaxy Evolution Explorer* (*GALEX*) found that 15% of SDSS ETGs display strong UV excess (Yi et al. 2005). Using *GALEX* UV imaging, Thilker et al. (2010) uncovered recent SF in the nearby ETG NGC 404, and showed that the UV light originates from recent SF activity through the analysis of archival images from the Hubble Space Telescope. The low-level SF observed in these galaxies is attributed to two mechanisms: external and internal (Méndez-Abreu et al. 2019; Davis et al. 2019), both of which can contribute significant amounts of gas to form new stars.

The external mechanism includes minor mergers with satellites or gas-rich dwarfs (Kaviraj et al. 2009; Thilker et al. 2010; Geréb et al. 2016), major mergers with gas-rich galaxies (McIntosh et al. 2014), accretion of metal-poor gas from the IGM (Finkelman et al. 2011), and cooling gas from the outer halo (Lagos et al. 2014). This external scenario brings in gas and reignites SF. One of the most obvious events is a merger with gas-rich galaxies or the accretion of material from the IGM. In both cases, the material accreted is likely to have a low metallicity (Davis & Young 2019).

The internal mechanism contains the stellar mass loss and cooling from the hot interstellar medium. Internal gas can be recycled to fuel low-level SF. The material of stellar mass-loss and/or gas from the hot phase of the

Corresponding author: Yu-zhong Wu  
yzwu@nao.cas.cn

interstellar medium (ISM, Sarzi et al. 2013) can cool in massive ETGs, and then reignite low-level SF (Pulido et al. 2018). The crucial feature of this mechanism is that the gas, coming from the inner halo, is metal-rich and shares the angular momentum of the stars (Davis & Young 2019).

In this work, we utilize integrated galaxy photometry from the catalog of the Wide-field Sky Survey Explorer (WISE, Wright et al. 2010). We apply a color cut of  $W2 - W3 < 2.5$  (where W2 and W3 are WISE bands, with central wavelengths of 4.6 and 12  $\mu m$ , respectively) to identify WISE-LSFR (low star formation rate) ETGs. These ETGs are selected from galaxies located in the section of the Baldwin-Phillips-Terlevich diagram (BPT, Baldwin et al. 1981) associated with H II regions or star forming regions. Approximately 27% of them exhibit a very low gas-metallicity relative to their stellar mass. Therefore, we investigate the properties of these ETGs. In section 2, we obtain the galaxy sample by utilizing the Data Release 7 (DR7; Abazajian et al. 2009) of the SDSS, and we use  $W2 - W3 < 2.5$  to derive the ETG sample from those galaxies. We present the properties of these ETGs, and study the main mechanism of metallicity dilution of our sample in Section 3. In Section 4, we summarize our results and conclusions. Through this work, we assume a flat cosmology with  $H_0 = 70 \text{ km s}^{-1} \text{ Mpc}^{-1}$ ,  $\Omega_M = 0.3$ , and  $\Omega_\Lambda = 0.7$ . We adopt a Chabrier (2003) initial mass function (IMF).

## 2. THE DATA

The data of the SDSS DR7 serve as the original sample of our study. Consequently, we employ the method of Wu, Zhang & Zhao (2019) to select our sample from the catalog of Max Planck Institute for Astrophysics – John Hopkins University (MPA-JHU) for the SDSS DR7. The catalog provides comprehensive measurements of emission line fluxes, SFRs (Brinchmann et al. 2004), and stellar masses (Kauffmann et al. 2003).

We select galaxies within the redshift range  $0.04 < z < 0.12$  to mitigate any bias arising from aperture effects (Kewley, Jansen & Gellar 2005) and the redshift evolution of the MZ relation (Zahid et al. 2013). For all galaxies in our sample, have a covering fraction of more than 20%, which is computed based on the fiber and petrosian magnitudes for the r band.

For these galaxies, we apply the following signal-to-noise (S/N) cuts of emission lines. Since the  $[\text{O III}]\lambda 5007$  line often appears in higher metallicity galaxies (Foster et al. 2012), applying an S/N cut to this line may introduce a bias in the metallicity measurements. Therefore, we require that the S/N ratio for  $\text{H}\alpha$ ,  $\text{H}\beta$ ,  $[\text{O II}]\lambda\lambda 3227, 3229$ , and  $[\text{N II}]\lambda 6584$  be greater than 3.

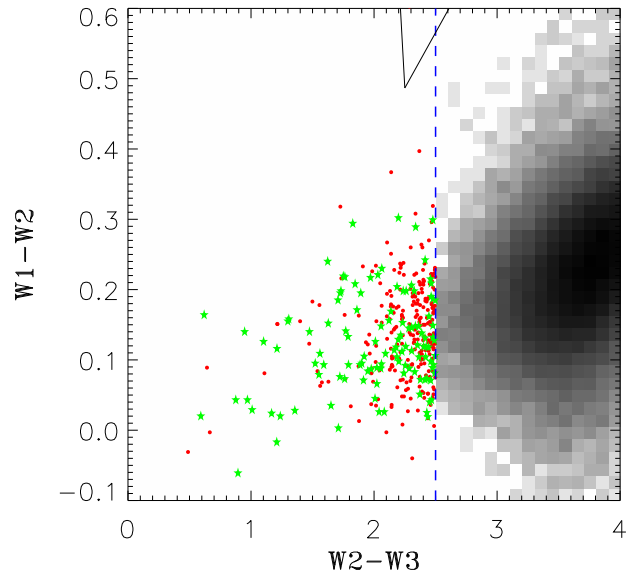


**Figure 1.** W2-W3 versus W1-W2 Diagnostic diagram. Black dots represent the galaxy sample with SF; red dots indicate galaxies without SF; green pentagrams are confirmed ETGs. The blue dashed line on this diagram demarcates the best boundary between galaxies with and without ongoing SF. The black lines delineate the ‘AGN’ wedge, as proposed by Mateos et al. (2012).

Using the BPT diagram (Baldwin et al. 1981), we select only those galaxies that fall within the H II region on this diagram (Kauffmann et al. 2003). Additionally, we ensure that the MPA-JHU catalog provides a measurement of the SFR for each galaxy. For the MPA-JHU SDSS DR7 catalog, we adjust for the difference in initial mass functions (IMFs) the Kroupa (2001) IMF assumed to the Chabrier (2003) IMF, applying a correction factor of 1.06. In total, 85,777 galaxies meet these criteria and constitute our sample.

In this work, we use the calibrator of T04 to estimate metallicities for our sample from the optical emission lines. We employ the  $R_{23}$  metallicity indicator to calculate the oxygen abundances of star-forming galaxies (SFGs, Pilyugin, Thuan & Vilchez 2006, 2010; Wu & Zhang 2013). The SFRs are taken from the MPA-JHU, based on the procedure described in Brinchmann et al. (2004), who used resolved imaging to obtain a method for aperture correction and estimated accurate measurements of the total SFRs in galaxies.

Here, the infrared data come from the WISE (Wright et al. 2010), with four bands: W1, W2, W3, and W4, corresponding to the central wavelengths of 3.4, 4.6, 12, and 22  $\mu m$ , respectively. In the WISE bands, W2 is dominated by stellar emission (e.g. Cluver et al. 2014), while W3 includes strong Polycyclic Aromatic Hydro-

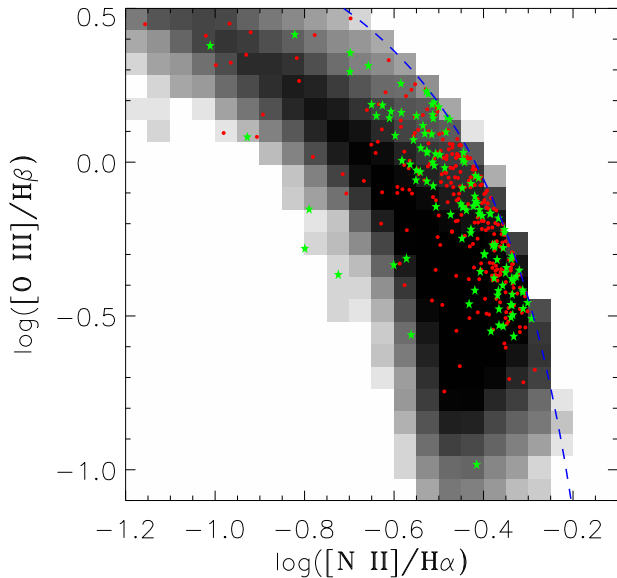


**Figure 2.** BPT Diagnostic diagram. The blue curve shows the Kauffmann et al. (2003) lower boundary for SFGs. Black dots indicate the galaxy sample with SF. The green pentagams are the same symbol as in Figure 1.

carbon emission bands, marking the appearance of SF-related warm dust (Herpich et al. 2016). Considering that the W2-W3 color is sensitive to warm dust powered by the SF region, we use the W2-W3 color index of  $> 2.5$  and  $< 2.5$  to distinguish galaxies with and without SF activity, respectively (Herpich et al. 2016). We cross-match the galaxy sample with the ALLWISE source catalog (doi: 10.26131/IRSA1) within  $2''$  and require  $S/N > 3$  for W2 and W3, resulting in a sample of 79,028 galaxies.

In this study, we first employ the criterion  $W2-W3 < 2.5$  to select WISE-LSFR galaxies from the above-mentioned galaxies, and then we identify ETGs from these galaxies, which satisfy the ETG condition. For the identification of ETGs, we adopt two criteria: a Sérsic index ( $n_{\text{Sersic}}$ ) greater than  $> 2.5$ , and an elliptical probability ( $p_e$ ) exceeding  $> 0.5$  (Herpich et al. 2018). The measurement of the  $n_{\text{Sersic}}$  indexes are sourced from the New York University Value-Added Galaxy Catalog (NYU-VAGC; Blanton et al. 2005). The elliptical probabilities are derived from *Galaxy Zoo 1* (Lintott et al. 2008, 2011), where volunteers used images of SDSS galaxies to categorize them into one of six types: edge-on, clockwise spiral, anticlockwise spiral, elliptical, star/do not know, or merger. Among the 79,028 galaxies, we apply the WISE-LSFR (defined by  $W2-W3 < 2.5$ ) and ETG (based on the sersic index and elliptical probability) criteria to obtain our final sample. (1) By us-

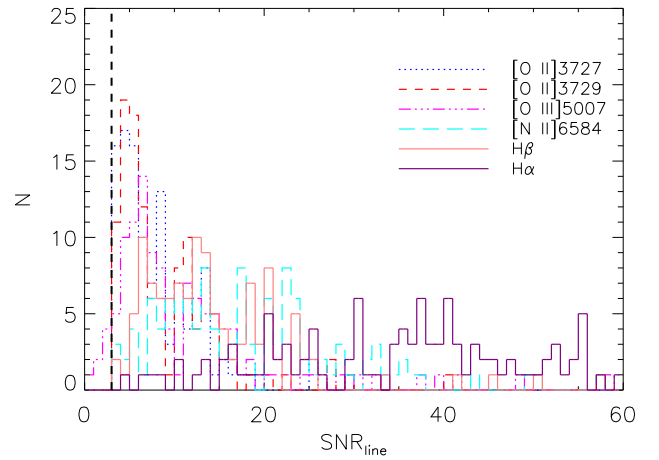


**Figure 3.** The distributions of SNRs for various emission lines. The different colors and line types represent SNRs corresponding to different emission lines within our sample. The thick black dotted line shows the  $SNR > 3$  of various lines.

ing  $W2-W3 < 2.5$ , we identify 391 WISE-LSFR galaxies from the initial sample. (2) By further applying the criteria  $p_e > 0.5$  and  $n_{\text{Sersic}} > 2.5$ , we ultimately obtain 117 ETGs that are both BPT-SF (star-forming, as indicated by their position in the H II region on the BPT diagram) and WISE-LSFR. These 117 galaxies possess three key characteristics: (1) they are located in the H II region on the BPT diagram, (2) they exhibit the WISE-LSFR property, and (3) they are classified as ETGs.

In this work, we have also used NUV, FUV, and r data to explore these galaxies. The NUV ( $\lambda_{\text{eff}} = 2267$ ) and FUV ( $\lambda_{\text{eff}} = 1528$ ) are provided by *GALEX*. These data originate from the NASA-Sloan Atlas catalog, which includes parameters and images of local galaxies derived from SDSS imaging and *GALEX* data. The NSA sample (v1\_0\_1) has approximately 640,000 galaxies. All the *GALEX* data used in this work can be accessed from MAST, doi: 10.17909/T9H59D. In our sample, the bluer W2-W3 color indicate lower star formation, whereas the SDSS spectrum displays SF in the BPT diagram, and they seem to be the apparent contradiction. Indeed, this is not surprising, since the WISE color is a global measure, while the SDSS spectrum represents the nuclear region. Therefore, we present and study the properties of 117 BPT-SF and WISE-LSFR ETGs.

### 3. RESULTS

#### 3.1. BPT-SF and WISE-LSFR early-type galaxies

In Figure 1, about 99.5% of the galaxies in 85777 SFG sample are star forming, while a minority of galaxies

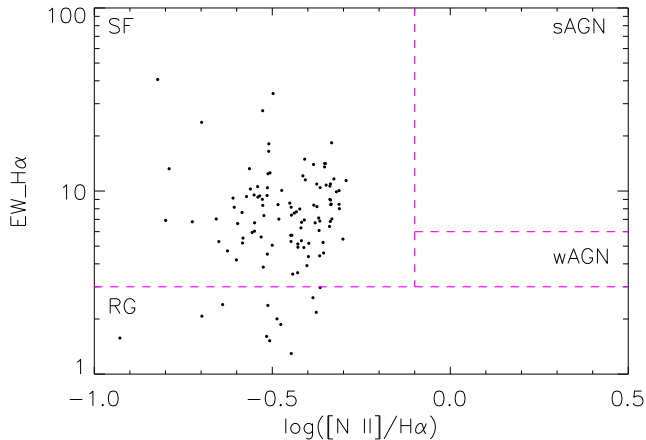


**Figure 4.** The WHAN diagram. The magenta lines demarcate the spectral classes suggested by Cid Fernandes et al. 2011.

without SF activity are located at the left of  $W2 - W3 = 2.5$  line. In this Figure, 391 galaxies are BPT-SF and WISE-LSFR galaxies, represented by red dots, and 117 BPT-SF and WISE-LSFR ETGs are represented by green pentagrams. None of these galaxies fall into the AGN region proposed by Mateos et al. (2012). For our ETG sample, we find that the majority of BPT-SF and WISE-LSFR ETGs possess relatively older stellar populations, which is associated with the fact that about 69% of these ETGs exhibit  $D_n4000 > 1.5$ . Given that these ETGs reside within the star-forming regions of on the BPT diagram, and they are selected using  $W2 - W3 < 2.5$ , which is a reliable diagnostic criterion for distinguishing galaxies with SF and without SF (Herpich et al. 2016), it is possible that low-efficiency SF activity still persists in these ETGs. Among the 117 BPT-SF and WISE-LSFR ETGs, their median redshift is  $\sim 0.07$ .

In Figure 6 of Herpich et al. (2016), they found that  $W2 - W3 = 2.5$  is the best separator between galaxies without SF and with ongoing SF. On the diagnostic diagram of  $W2 - W3$  versus  $W1 - W2$ , most of our galaxy with the WISE data lie to the right of the blue dashed line ( $W2 - W3 = 2.5$ ). In Wu (2020), they also utilized this color to show a separation between the ETG sample with SF and without SF, and they measured the metallicities of these ETGs with SF. In our galaxy sample, Figure 1 describes that almost all of these galaxies have SF activities, and we identify a special sample with low-SFR through the  $W2 - W3 = 2.5$  color.

In Figure 2, we present the galaxy sample on the BPT diagram. The blue dashed curve represents the lower limit for SFGs as defined by Kauffmann et al. 2003. The green pentagrams highlight BPT-SF ETGs

with  $W2 - W3 < 2.5$ . We find that most galaxies with  $W2 - W3 < 2.5$  (shown as red dots) approach the blue line. Notably, a majority of BPT-SF and WISE-LSFR ETGs are also located close to the blue dashed curve in Figure 2. This indicates that galaxy samples exhibiting weak SF activity tend to sit closer to the SFG lower limit of Kauffmann et al. (2003). Actually, this proximity may stem from the fact that SFGs in general, can receive a contribution from LINERs (low ionization nuclear emission-line region) given their typically low  $EW_{H\alpha}$  (the  $H\alpha$  equivalent width).

For the spectra of our sample, we reanalyze the various emission lines for 117 ETG sample. Figure 3 shows the distributions for SNRs for the six emission lines. For the emission lines of  $H\alpha$ ,  $H\beta$ ,  $[O II]\lambda\lambda 3727, 3729$ , and  $[N II]\lambda 6584$ , we note that the SNRs of the five emission lines are greater than 3, while proportions of their SNRs being greater than 6 are greater than 92%. For  $[O III]\lambda 5007$ , we select galaxies with  $SNR > 2$ , which does not have much influence on the results of this work. On the one hand, for ETGs, their emission lines are very weak, and the limitation of SNR has a significant impact on the sample size, directly reducing the number of samples; on the other hand, although the SNR reduces the sample size, it can ensure the accuracy of sample classification results. Therefore, the SNR of  $[O III]\lambda 5007$  emission line is chosen to be greater than 2. 97%(110/114) of our sample have SNRs greater than 3, while 76%(84/114) of the 114 ETGs have SNR greater than 6. From these analyses of these emission lines, we confirm well-detected emission lines and the BPT classification for our sample.

We also explore the equivalent width of  $H\alpha$  in star-forming regions for our sample. 89%(101/114) of the 114 ETGs have  $EW_{H\alpha} > 3 \text{ \AA}$ , while 66%(75/114) of our sample have  $EW_{H\alpha} > 6 \text{ \AA}$ . Cid Fernandes et al. (2011) suggested that star-forming regions exhibit  $EW_{H\alpha} > 3 \text{ \AA}$ . In addition, we should consider our sample may be contaminated by LINER emission. Therefore we present 114 ETGs on the WHAN diagram in Figure 4. According to the galaxy classification of Cid Fernandes et al. (2011), AGNs with  $3 \text{ \AA} < EW_{H\alpha} < 6 \text{ \AA}$  are classified as weak AGNs (wAGNs), while AGNs with  $EW_{H\alpha} > 6 \text{ \AA}$  are strong AGNs (sAGNs). From Figure 4, LINERs are located in the wAGN region on the WHAN diagram, indicating that our sample may not be significantly affected by wAGN contamination. Consequently, we can ensure that the line ratios are also not contaminated by LINER emission, allowing us to obtain reliable metallicity measurements.

In Figure 5, we show the relations of stellar mass versus  $12 + \log(O/H)$  and u-r color for BPT-SF and WISE-

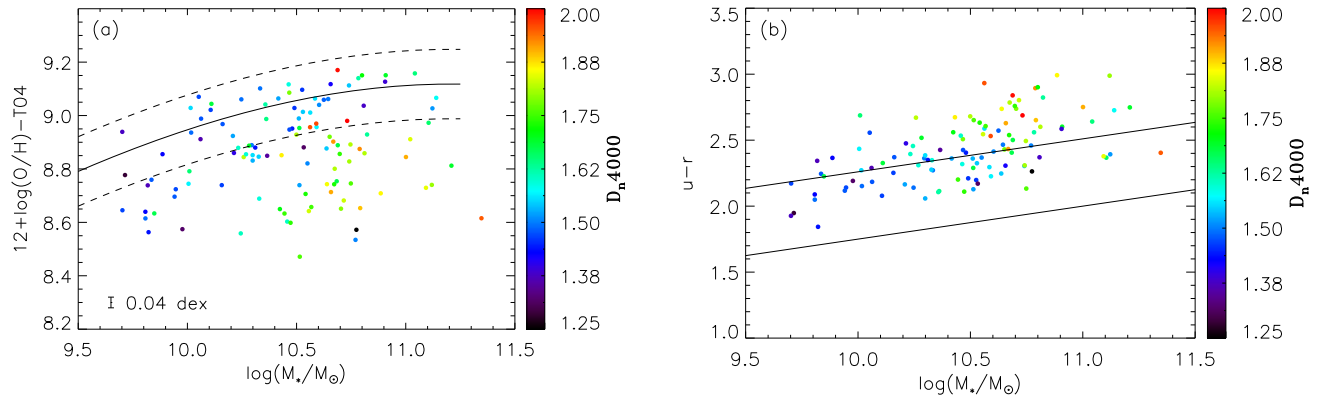


**Figure 5.**  $12+\log(\text{O}/\text{H})$  and  $u-r$  color vs. the stellar mass with the color bar of  $D_n4000$ . Left-hand panel: the stellar mass vs.  $12+\log(\text{O}/\text{H})$ . The black solid and dashed curves represent the MZ relation and its  $1\sigma$  scatter of Tremonti et al. (2004). Right-hand panel: the stellar mass vs.  $u-r$  color. The location of the green valley galaxies is indicated with the two solid lines (Schawinski et al. 2014).

LSFR ETGs using the color bar of  $D_n4000$ . In Figure 5(a), the black solid curve is the MZ relation from Tremonti et al. (2004), and the black dashed lines represent its  $1\sigma$  scatter. In Davis & Young (2019), 7.4% (42/567) of their ETGs represents metallicities exceeding more than 2 standard deviation (0.26 dex) below the Tremonti et al. (2004) MZ relation. In contrast, 28% (32/114) of our ETG sample deviates by at least 0.26 dex below the Tremonti et al. (2004) MZ relation. Furthermore, 56% (64/114) of our ETG sample falls not less than 1 standard deviation below the MZ relation of Tremonti et al. (2004). These findings indicate that our BPT-SF and WISE-LSFR ETG sample has a significantly higher percentage of galaxies exceeding 0.26 dex below the Tremonti et al. (2004) relation, approximately 3.8 times higher than the sample of Davis & Young (2019). In addition, we find that quite a few of these ETGs, which deviated by more than  $1\sigma$  standard deviation below the MZ relation of Tremonti et al. (2004), possess an older stellar population and higher stellar mass. Compared to the metallicity difference at lower stellar mass, these galaxies with higher stellar masses show larger metallicity differences and older stellar population.

When comparing the metallicity of ETGs and late-type galaxies (LTGs, also known as SFGs) at a fixed galaxy stellar mass, it is feasible that a statistical analysis, facilitated by the combination of theoretical models of galaxy formation and evolution with extensive data samples derived from numerous observations of these two galaxy types, has the potential to reveal their metallicity variations and the underlying causes of these differences. In Davis & Young (2019), they used a large

sample of ETGs to explore the origin of the gas that fuels RSF and considered the effect of accretion of metal-poor gas on ETGs. In this article, we also utilize a large sample of ETG data, in conjunction with theories related to galaxy evolution, to analyze the lower metallicity exhibited by some galaxies within our sample, and to delve into the possible reasons behind this phenomenon.

With regard to those ETGs with ultra-low metallicity, we have calibrated them using alternative strong line metallicity indicators, specifically the calibrators from Dopita (2016) and Sanders et al. (2018). Our findings indicate that these ETGs still have lower metallicities, confirming the reliability of their ultra-low metallicity status. When we excluded the criterion  $W2-W3=2.5$  and select ETGs solely based on  $p_e > 0.5$  and  $n_{\text{seraic}} > 2.5$ , we obtain 2530 ETGs. Among these, 5.1% (130/2530) exhibit metallicities that are more than  $12+\log(\text{O}/\text{H})=0.26$  dex below the MZ relation of Tremonti et al. (2004). Notably, this percentage is lower than that reported in Davis & Young (2019). Furthermore, we observe that the percentage of ETGs selected with the  $W2-W3$  cut is about 5.5 times higher than that without the cut. This suggests that the discrepancy between our work and Davis & Young (2019) may stem from the fact that our ETGs, selected based on the  $W2-W3$  color, tend to have lower SFRs compared to the sample used in Davis & Young (2019).

Figure 5(b) shows the relation of stellar mass and  $u-r$  color with the color bar of  $D_n4000$ . The two black solid lines represent the green valley galaxies on the stellar mass versus  $u-r$  color diagram, and come from equations (1) and (2) of Schawinski et al. (2014). From Figure 5(b), 67 ETGs locate in the red cloud, and more than

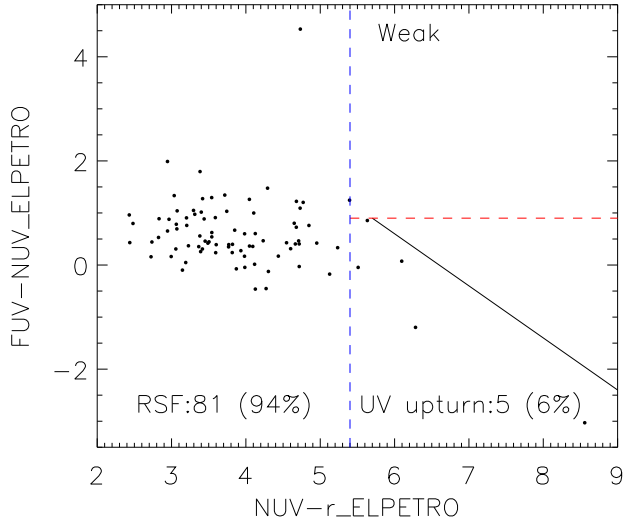


**Figure 6.** Two-color diagram for RSF and UV upturn classification for our ETG sample (Yi 2011). The red horizontal dashed line represent a rising UV slope, the blue vertical dashed line denotes the criterion for identifying young stars, and the slanted solid line indicates the UV strength required for a galaxy to be classified as a UV upturn galaxy. RSF stands for residual SF.

half of them have an older stellar population ( $D_n4000 \gtrsim 1.5$ ), while 47 ETGs lie in the green valley region. This shows that these ETGs with an older stellar population, higher stellar mass, and larger metallicity deviation from the MZ relation tend to have a redder color.

In Figure 6, we exhibit residual star formation (RSF) of our sample ETGs in the NUV-r versus FUV-NUV diagram. Due to that NUV has a high sensitivity for the presence of young stars, it is used to explore SF activity in ETGs. In fact,  $\text{NUV-r} \leq 5.4$  is the most frequently used criterion to identify ETGs with RSF, and about 94 percent (81/86) of our sample galaxies met the condition. Based on the *GALEX* and SDSS data, Jeong et al. (2022) suggested that the RSF of the sample may be from external processes (i.e. mergers or interaction), even if these ETGs are quiescent today.

In Figure 7, we show the diagram of stellar mass and SFR for BPT-SF and WISE-LSFR ETGs. The black dotted-dashed line is the best fit for the SDSS data from Renzini & Peng (2015). 114 ETGs are represented by the black dots in Figure 7. Figure 7 displays a clear correlation, indicating that galaxies with lower stellar masses tend to have lower SFRs, while those with higher stellar masses tend to have higher SFRs. Almost all of the ETGs locate below the fit line, except for 2 ETGs, and these ETGs lie below the main sequence of SFGs by an average of 0.8 dex, showing that these ETGs exhibit

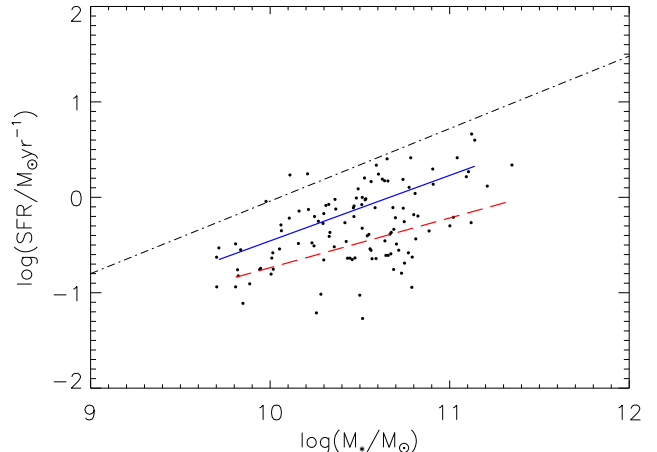


**Figure 7.** Diagram of the stellar mass and SFR for our ETG sample. The black dotted-dashed line represents the best fit to the SDSS data (Renzini & Peng 2015). The green pentagrams are the same symbol as in Figure 1. The blue solid and red dashed lines exhibit the best least-squares fits for the two samples, with the fits located within  $1\sigma$  region and below  $2\sigma$  level of the MZ relation.

weaker SFRs. This may be because the W2-W3 color acts as a cut on the SFR –  $M_*$  diagram to remove galaxies with higher SFRs on the main sequence, and the remaining galaxies generally have lower SFRs. Also, we obtain the best least-squares fit  $\log(\text{SFR}/(\text{M}_\odot \text{yr}^{-1})) = (0.55 \pm 0.09)\log(M_*/\text{M}_\odot) - (6.08 \pm 0.96)$  for our 114 ETGs. Compared with the star-forming ETG sample of Wu & Zhang (2021), our sample has a significantly lower slope in the SFR-stellar mass relation. In addition, the blue solid and red dashed lines represent the best least-squares fits for the two samples, lying within the  $1\sigma$  region and below the  $2\sigma$  standard deviation of the MZ relation in Figure 5(a), respectively. This indicates that at a given stellar mass, ETGs with higher SFRs tend to have relatively higher metallicity.

### 3.2. Dilution effect and low-level SF in BPT-SF and WISE-LSFR ETGs

In the local study of Lagos et al. (2014), they found that gas accretion from minor mergers contributes neutral gas in 8% of ETGs at  $z = 0$ , while cooling gas from the hot halos contributes the gas in  $\approx 90\%$  of ETGs (depending on some model parameters). In fact, the most massive galaxies of ETGs tend to host the largest hot halos (e.g., Goulding et al. 2016). With regard to the scheme of hot halo cooling, we examine the large-scale environment of our ETGs. In Figure 8, we describe the number distributions of galaxies in galaxy clusters. The galaxy group for our ETG sample is based on the halo-

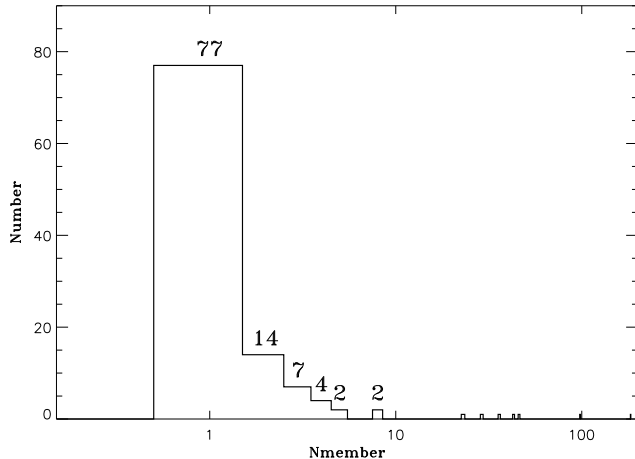


**Figure 8.** Number distributions of galaxies in galaxy groups. The histograms indicate the distributions derived from the galaxy group sample in the SDSS.

based group finder developed by Yang et al. (2007), and we obtain group membership of 113 galaxies for our ETGs. When its value is 1, it can be considered to be in an isolated environment. Therefore, the vast majority of galaxies (77/114) in our sample are in an isolated environment. Figure 8 shows that most of our sample is composed of field galaxies, indicating that metallicity dilution may not be induced by the hot halo cooling. In addition, Figure 8 displays these ETGs inhabit a low-density environment (LDE), judged by the number of candidate companions, and LDE typically hosts ETGs that are “young and active” compared to their cluster counterparts (Clements et al. 2009).

Minor mergers are more common and trigger SF activity in the local Universe (Kaviraj et al. 2009, 2014), while major mergers are more usual at high redshift (Conselice et al. 2003). In a sample of 42 outliers from the MZ relation of SFGs, Peeples, Pogge & Stanek (2009) proposed the tidal interaction inducing gas inflow results in their lower metallicities. In massive SFG sample, Sol Alonso, Michel-Dansac & Lambas (2010) also found low metallicity and high stellar mass, and suggested that merger-induced less enriched gas inflows produce the result. In the two merging galaxies of NGC4809/4810, Gao et al. (2023) found that star formation activities are triggered by the merger of two dwarf galaxies at the interaction area, and star-forming knots present poor metallicity, which may be the dilution of deficient-poor gas inflows during the merging event of the two galaxies. Figure 5(a) shows the dilution effect significantly, and these massive ETGs have decreased  $\sim 0.2 - 0.5$  dex in metallicity compared with

the MZ relation of Tremonti et al. (2004) at the same stellar mass.

The star formation in ETGs may originate from recent interactions or mergers, and indicative features of these events include shells, stellar streams, and tails. Several papers have shown that shells, tails, and ripples represent signatures of merging events (Tal et al. 2009; Duc et al. 2015; Rampazzo et al. 2020; Mancillas et al. 2019). George (2023) supposed that star formation in blue early-type galaxies represents a stage in the evolution of ETGs. These features will eventually vanish, and star formation associated with these events will cease, allowing the galaxy to transition into another stage of ETGs (George 2023). In our sample, while some signatures of merging events in some ETGs may have disappeared, merger-induced star formation in these ETGs has indeed occurred. Therefore, gas inflow induced by mergers and interactions is one of the important reasons for lower metallicities in galaxies.

Because misalignment of stellar and gas rotation in galaxies reveals the origin and processing of accreted gas, the fresh gas has more chances to appear and be accreted in ETGs, and accreted external fresh material may be a cause of lower SF (Davis et al. 2014; van de Voort et al. 2018). From observations of 1,213 galaxies of the Sydney-AAO Multi-object Integral field spectrograph galaxy survey, Bryant et al. (2019) also found that the misalignment fraction is  $45 \pm 6\%$  in ETGs. Using the MaNGA data, Lee et al. (2023) found that star formation activity in star-forming/blue ETGs comes from an external origin, including accretion gas from the IGM or galaxy mergers. Based on a finding that the stellar metallicity of ETGs is larger than their gas-phase metallicity, Davis & Young (2019) suggested that this dilution material comes from an external source. The redshift range of our sample is  $0.04 < z < 0.12$ , falling within the sample redshift of Davis & Young (2019). Our sample has the lowest SFR of  $0.05 M_{\odot} \text{ yr}^{-1}$ , and the median value is  $0.5 M_{\odot} \text{ yr}^{-1}$ . Our smaller sample likely overlaps with their sample, and therefore we suggest that the fresh gas, accreted by some ETGs in our ETG sample, may also come from the IGM. These indicate that the accreted fresh gas from the IGM may be one of the important reasons for lower metallicities in galaxies.

The massive ETGs often have smaller  $M_{\text{gas}}/M_{*}$  ratios ( $M_{\text{gas}}$  is the mass of gas, Young et al. 2014), and the inflow gas may easily dilute their gas-phase metallicity. In this study, BPT-SF and WISE-LSFR ETGs with older stellar populations may have a lower metallicity of ISM than ETGs with younger stellar populations, and these older galaxies need less fresh material to dilute

their metallicities than younger ones at the same stellar mass. We can see that BPT-SF and WISE-LSFR ETGs with older stellar populations may be more easily diluted than those with younger stellar populations, and most of these ETGs exceed 1 standard deviation below the Tremonti et al. (2004) MZ relation. Moreover, some of BPT-SF and WISE-LSFR ETGs with younger stellar populations also exceed 1 standard deviation in Figure 5(a), and this may be due to infalling low-metallicity gas from the external sources having different masses, resulting in different dilution effects and thus these metallicity differences.

Moreover, Figure 5 shows that galaxies with the higher stellar mass tend to have older stellar populations, redder colors, and larger metallicity deviations from the Tremonti et al. (2004) MZ relation. Although we use  $W2-W3 < 2.5$  to select our galaxies, this color threshold primarily serves to distinguish those without significant SF. Consequently, our sample may encompass a transition from galaxies with weaker SF to those without SF. These ETGs lacking SF may have experienced the inflow of external gas, diluting their gas-phase metallicity, but not start triggering SF. In this context, our sample may include galaxies with lower metallicity and lower SFR, while those with just-ceased SF activity may exhibit higher metallicity and higher SFR. Using 1575 MaNGA data, Sharma et al. (2023) found 83 galaxies with HI rich and low SFR, suggesting that a recent accretion of HI gas, without igniting SF, may be one of the key factors underlying this phenomenon.

The cold gas flow can result in the metallicity decreasing. Some galaxies that hold much gas may experience star formation, and their metallicity shows a relatively small decrease, when external fresh gas inflows. Other galaxies that have little gas may have less SF, and their metallicity exhibits a significant decrease, when external gas inflows. The two processes may correspond to our two samples in Figure 5(a), with the first one falling within the  $1\sigma$  region of the Tremonti et al. (2004) MZ relation in Figure 5(a), while the second one may lie below the  $2\sigma$  standard deviation of the MZ relation. Actually, not all inflows of low-metallicity material enter and trigger SF events, and the probability of this occurring is often small. For these older massive ETGs with lower gas content, a small mass of low-metallicity gas may dilute the metallicity considerably (Belfiore et al. 2015; Wu 2022). In addition, we demonstrate the distribution fits of the two samples in Figure 7, with the fits of the first and second samples corresponding to the blue solid and red dashed lines, respectively. Compared with ETGs with higher metallicity, ETGs with lower metallicity are further away from the “main sequence” of SFGs, and

thus often have lower SFR. This directly supports the dilution effect of metallicity deviation shown in Figure 5. Therefore, we suggest that these ETGs with metallicity dilution might be attributed to the inflow of metal-poor gas from mergers/interaction or the IGM.

#### 4. SUMMARY

In this study, we use  $W2-W3=2.5$  as the diagnostic tool to derive the observational data of 114 BPT-SF and WISE-LSFR ETGs, which cross-match the *Galaxy Zoo 1* with the galaxy sample from the catalog of the SDSS DR7 MPA-JHU emission-line measurements. We explore the properties of these BPT-SF and WISE-LSFR ETGs. We summarize our results as follows:

1. We find that  $\sim 28\%$  (32/114) of BPT-SF and WISE-LSFR ETGs exhibit a metallicity deviation of at least 2 standard deviation (0.26 dex) below the MZ relation of Tremonti et al. (2004).

2. We note that almost all of BPT-SF and WISE-LSFR ETGs lie below the “main sequence” of SFGs proposed by Renzini & Peng (2015) in the SDSS data, which may be because the  $W2-W3$  color is a cut on the  $SFR-M_*$  diagram to remove galaxies with higher SFRs on the SFG Main-Sequence.

3. We find that a majority of BPT-SF and WISE-LSFR ETGs sit closer to the SFG lower limit of Kauffmann et al. (2003). This may indicate that ETGs with weak SF activity may receive a contribution from LINERs given their generally low  $EW_{H\alpha}$ . In addition, these massive BPT-SF and WISE-LSFR ETGs tend to have redder color.

4. As depicted in Figure 7, ETGs with a larger deviation in metallicity from the MZ relation of Tremonti et al. (2004) often exhibit lower SFRs, which reinforces the observed metallicity dilution shown in Figure 5.

5. From the number distributions of galaxies in a group, most of 114 ETGs are field galaxies, and this implies that the metallicity dilution of our ETGs may not be induced by the hot halo cooling.

6. We suggest that the dilution effect may be attributed to the inflow of metal-poor gas from mergers/interaction or the IGM, and that low-level SF in most of 114 ETGs may be attributed to the accretion of fresh gas in the local massive ETGs.

#### ACKNOWLEDGMENT

We thank the anonymous referee for valuable suggestions and comments, which helped us to improve the paper significantly. This work is supported by the NSFC (No. 12090041, 12090040) and the National Key



R/&D Program of China grant (No. 2021YFA1600401; 2021YFA1600400).

## REFERENCES

- Abazajian, K. N., Adelman-McCarthy, J. K., Agüeros, M. A. et al. 2009, *ApJS*, 182, 543
- Baldwin, J. A., Phillips, M. M., & Terlevich, R. 1981, *PASP*, 93, 5
- Belli, S., Genzel, R., Forster, D. J. et al. 2017, *ApJL*, 841, L6
- Blanton, M. R., Schlegel, D. J., Strauss, M. A., et al. 2005, *AJ*, 129, 2562
- Brinchmann, J., Charlot, S., White, S. D. M., et al. 2004, *MNRAS*, 351, 1151
- Bryant, J. J., Croom, S. M., van de Sande, J., et al. 2019, *MNRAS*, 483, 458
- Chabrier, G. 2003, *PASP*, 115, 763
- Cid Fernandes, R., Stasinska, G., Mateus, A., & Vale Asari, N. 2011, *MNRAS*, 413, 1687
- Clements, M. S., et al. 2009, *MNRAS*, 392, L35
- Cluver, M. E., Jarrett, T. H., Hopkins, A. M., et al. 2014, *ApJ*, 782, 90
- Conselice, C., Bershady, M. A., Dickinson, M., & Papovich, C. 2003, *AJ*, 126, 1183
- Davis, T. A., Greene, J. E., Ma, Chung-Pei., et al. 2019, *MNRAS*, 486, 1404
- Davis, T. A., & Young, L. M. 2019, *MNRAS*, 489, L108
- Davis, T. A., Young, L. M., Crocker, A. F., et al. 2014, *MNRAS*, 444, 3427
- Dopita, M. A. 2016, *APSS*, 361, 61
- Duc, P., et al. 2015, *MMRAS*, 446, 120
- Finkelman, I., Moiseev, A., Brosch, N & Katkov, I. 2011, *MNRAS*, 418, 1834
- Foster, C., et al. 2012, *A&A*, 547, A79
- Gao, Y. L., Gu, Q. S., Liu, G. L., et al. 2023, *A&A*, 677, A179
- George, K. 2023, *A&A*, 678, A10
- Geréb, K., Catinella, B., Cortese, L., Bekki, K., Moran, S. M & Schiminovich, D. 2016, *MNRAS*, 462, 382
- Goulding, A. D., et al. 2016, *ApJ*, 826, 167
- Herpich, F., Mateus, A., Stasińska, G., Cid Fernandes, R., & Vale Asari, N. 2016, *MNRAS*, 462, 1826
- Herpich, F., Stasińska, G., Mateus, A., Vale Asari, N., & Cid Fernandes, R. 2018, *MNRAS*, 481, 1774
- Jeong, H., Oh, K, Joo, S. J., & Yi, S. K. 2022, *MNRAS*, 509, 550
- Kauffmann, G., Heckman, T. M., Tremonti, C., et al. 2003, *MNRAS*, 346, 1055
- Kaviraj, S. 2014, *MNRAS*, 437, L41
- Kaviraj, S., Schawinski, K., Devriendt, J. E. , et al. 2007, *ApJS*, 173, 619
- Kaviraj, S., Sebastien, P., Khochfar, S., Silk, J & Kay, S. 2009, *MNRAS*, 394, 1713
- Kewley, L. J., Jansen, R. A., & Geller, M. J. 2005, *PASP*, 117, 227
- Kroupa, P. 2001, *MNRAS*, 322, 231
- Lagos, C. d. P., Davis T. A., Lacey, C. G., et al. 2014, *MNRAS*, 443, 1002
- Lee, Y. H., Hwang, H. W., Hwang, N., Lee, J. C., & Kim, K. B. 2023, *ApJ*, 953, 88
- Lequeux, J., Peimbert, M., Rayo, J. F., Serrano, A., & Torres-Peimbert, S. 1979, *A&A*, 80, 155
- Lintott, C. J., Schawinski, K., Bamford, S., et al. 2011, *MNRAS*, 410, 166
- Lintott, C. J., Schawinski, K., Slosar, A., et al. 2008, *MNRAS*, 389, 1179
- Mancillas, B., et al. 2019, *A&A*, 632, A122
- Mateos, S., Alonso-Herreo, A., Carrera, F. J., et al. 2012, *MNRAS*, 426, 3271
- McIntosh, D. H., Wagner, C., Cooper, A., et al., 2014, *MNRAS*, 442, 533
- Méndez-Abreu, J., Sánchez, S. F., & de Lorenzo-Cáceres, A. 2019, *MNRAS*, 488,L80
- Peeples, M. S., Pogge, R. W., & Stanek, K. Z. 2009, *ApJ*, 695, 259
- Pilyugin, L. S., Thuan, T. X., Vílchez, J. M. 2006, *MNRAS*, 367, 1139
- Pilyugin, L. S., Vílchez, J. M., Cedrés, B., Thuan, T. X. 2010, *MNRAS*, 403, 896
- Pulido, F. A., McNamara, B. R., Edge, A. C., et al. 2018, *ApJ*, 853, 177
- Rampazzo, R., et al. 2020, *A&A*, 640, A38
- Renzini, A., & Peng, Y.-J. 2015, *ApJL*, 801, L29
- Sanders, R. L., Shapley, A. E., Kriek, M., et al. 2018, *ApJ*, 858, 99
- Sarzi, M., et al. 2013, *MNRAS*, 432, 1845
- Schawinski, K., Urry, C. M., Simmons, B. D., et al. 2014, *MNRAS*, 440, 889
- Sharma, A., Masters, K. L., Stark, D. V., et al. 2023, *MNRAS*, 526, 1573
- Sol Alonso, M., Michel-Dansac, L., & Lambas, D. G. 2010, *A&A*, 514, A57
- Tal, T., et al. 2009, *ApJ*, 138, 1417

- Thilker, D. A., Bianchi, L., Schiminovich, D., et al. 2010, ApJL, 714, 171
- Tremonti, C. A., Heckman, T. M., Kauffmann, G., et al. 2004, ApJ, 613, 898
- van de Voort, F., Davis, T. A., Matsushita, S., et al. 2018, MNRAS, 476, 122
- Wright, E. L., Eisenhardt, P. R. M., Mainzer, A. K., et al. 2010, AJ, 140, 1868
- Wu, Y.-Z. 2020, ApJL, 893, L33
- Wu, Y.-Z., Zhang, S.-N. 2013, MNRAS, 436, 934
- Wu, Y.-Z., & Zhang, W. 2021, MNRAS, 503, 2340
- Wu, Y.-Z., Zhang, W., & Zhao, Y.-H. 2019, MNRAS, 486, 5310
- Yang, X.-H., Mo, H. J., van den Bosch, F. C., et al. 2007, ApJ, 671, 153
- Yi, S. K., et al. 2005, ApJ, 619, 111
- Yi, S. K., Lee, J., Sheen, Y.-K., et al. 2011, ApJS, 195, 22
- Young, L. M., Scott, N., Serra, P., et al. 2014, MNRAS, 444, 3408
- York, D. G., et al. 2000, AJ, 120, 1579
- Zahid, H. J., Geller, M. J., Kewley, L. J., et al. 2013, ApJ, 771, 19